Original Research

Desorption and Competitive Adsorption of Mn²⁺ and Cd²⁺ from Acidic Wastewater by RM-L73

Yisi Lu[1, 2]*, Hao Ma[1], Yutao Ma[1], Dongru Guo[1], Xiaofeng Liu[2]

[1]Yellow River Engineering Consulting Co., Ltd., No. 109 Jinshui Road, Jinshui District,
Zhengzhou, Henan, 450003, China
[2]College of Civil Engineering, Taiyuan University of Technology, No.79 West Yingze Street,
Taiyuan, Shanxi, 030024, China

Abstract

This study investigated the desorption characteristics of red mud and loess with an optimum mass ratio (RM-L73) loaded with Mn²⁺ and Cd²⁺ in neutral and acidic environments through batch desorption tests. The desorption mechanism was clarified by understanding the capture mechanism of RM-L73 and establishing desorption isotherms. Furthermore, the effect of coexisting ions on RM-L73's removal efficiency was examined by batch adsorption tests. Results indicate that the -OH groups in RM-L73 play a substantial role in capturing Mn²⁺ and Cd²⁺ from acidic wastewater and considerably enhance the adsorption effect of RM-L73. Additionally, Cd²⁺ was more sensitive to environmental pH levels than Mn²⁺, and a desorption distribution coefficient was introduced to characterize the ease of desorption. Coexisting ions had antagonistic effects on the removal of Mn²⁺ and Cd²⁺. The inhibitory effect generally intensified with increasing initial concentration of Cd²⁺. However, the inhibitory effect on Mn²⁺ could be mitigated at high concentrations. Cu²⁺ significantly reduced the adsorption capacity of RM-L73 for Mn²⁺ and Cd²⁺, with a stronger effect on Mn²⁺.

Introduction

Acid mine drainage is recognized by the U.S. Environmental Protection Agency (US-EPA) as one of the three major ecological risks [1]. The acid mine drainage continuously generated by abandoned coal mines, if not effectively and properly treated and improved, results in a large amount of acidic wastewater containing heavy metal ions that may directly enter groundwater and surface water, causing irreversible impacts on the ecological environment and even endangering human health [2-4]. Nearly 8780 closed coal mines in Shanxi Province of China, a large number of abandoned mines and tailings in the Witwatersrand Basin of South Africa, and approximately 2260 abandoned mines in Canada have been submerged by acid mine drainage. These continuous generations of acid mine drainage pose a serious threat to the ecological security of watersheds and regions [5-7]. Exploring effective treatment approaches for soil and water environmental pollution caused by acid mine drainage has always been a focal point and global

---

*e-mail: luyisityut@163.com, luyisi@yrec.cn
Tel.: +86-0371-66021030 F

challenge. Scholars have explored various approaches to wastewater treatment. For example, biochar produced through co-hydrothermal carbonization of biomaterials and the nanomaterials synthesized using either inorganic or organic materials [8-12] are among the technologies being explored.

Acid mine drainage is widely generated in coal mining areas in China, particularly in Shanxi Province, a major coal-producing region. The pH of acid mine drainage is generally between 2.0 and 3.0, and it contains pollutants that exceed standards, including Mn^{2+}, Fe^{2+}, Fe^{3+}, Zn^{2+}, Cd^{2+}, and Cu^{2+} [13, 14]. Mn^{2+} and Cd^{2+}, as heavy metal ions with high activity and mobility, have become the focus of this study. Mn^{2+} can harm aquatic and terrestrial ecosystems and lead to iron deficiency in algae, acute toxicity in fish, and embryonic death. In humans, excessive consumption of Mn^{2+} can lead to seizures and potentially permanent neurological disorders and affect respiration, reproduction, and development. Long-term exposure to high concentrations of Mn^{2+} can also result in neurological syndromes characterized by cognitive, mental, and motor abnormalities and increased risk of developing specific forms of Parkinson's disease [15, 16]. Cd^{2+}, which has high mobility and strong accumulation capabilities, is classified as a Class I carcinogen by the International Agency for Research on Cancer. Additionally, Cd^{2+} has toxic effects on the lungs, kidneys, and bones. Excessive exposure to Cd^{2+} may also lead to overflow proteinuria and disruption of potassium metabolism in urine [17-19].

Currently, common methods for treating acid mine drainage globally include ion exchange, adsorption, permeable membrane processes, chemical treatments, microbial remediation, and artificial wetland systems [20-23]. Adsorption has gained widespread application due to its minimal generation of secondary pollution [24-26]. In recent years, the resource utilization of industrial solid waste has gained favor in the field of heavy metal adsorption [27-29]. In our preliminary research results, the red mud and loess mixture with a mass ratio of 7:3, RM-L73, possesses satisfactory pH buffering ability and adsorption capacity for acidic wastewater containing Mn^{2+} and Cd^{2+} [30, 31]. Adsorption is the process by which target ions are captured and held onto the adsorbent, whereas desorption refers to the release of target ions from the adsorbent that has already bound the pollutant. Desorption is essentially the reverse process of adsorption. The greater the desorption amount, the weaker the ability of the adsorbent to adsorb and retain target ions, making them more likely to be re-released into the liquid phase as ions. This consequence could potentially re-contaminate the water and soil environment [32]. Therefore, the safety and stability of employing RM-L73 to purify acid mine drainage requires further evaluation. The desorption characteristics of target ions on RM-L73 are crucial for assessing the safety of RM-L73 loaded with target ions, as well as for proper disposal and recovery of heavy metals. Additionally, heavy metal ions in actual acid mine drainage coexist with multiple other ions rather than existing in isolation. Therefore, the competitive behavior among multiple heavy metal ions is essential for further evaluating the stability and effectiveness of the adsorbent.

This study investigates the desorption characteristics of RM-L73 loaded with Mn^{2+} and Cd^{2+} in both neutral and acidic environments. Furthermore, the safety and effectiveness of RM-L73 are evaluated. Additionally, the competitive adsorption characteristics of target ions in binary and ternary systems are systematically studied where other heavy metal ions are present. The selective adsorption sequence of RM-L73 for heavy metal ions is obtained, and the intrinsic mechanism of competitive adsorption is explored to provide theoretical guidance for the application of RM-L73.

Materials and Methods

Materials

RM-L73

The Bayer process red mud from the Shanxi Liulin Aluminum Plant was used in this study. The loess belongs to the late Quaternary sediment (Q4), which was collected from approximately 4-5 m underground at a construction site in the Dongshan area of Taiyuan (Shanxi, China). The red mud and loess were mixed in a mass ratio of 7:3 and stored for future use. The main chemical components and contents of red mud and loess are detailed in the following information: red mud (Al_2O_3: 24.34%; SiO_2: 20.17%; CaO: 18.26%; Fe_2O_3: 9.40%; MgO: 1.26%; K_2O: 0.64%; Na_2O: 9.61%; TiO_2: 3.56%; SO_3: 0.47%; MnO: 0.03%), loess (Al_2O_3: 11.75%; SiO_2: 58.88%; CaO: 7.98%; Fe_2O_3: 4.54%; MgO: 2.05%; K_2O: 2.18%; Na_2O: 1.70%; TiO_2: 0.60%; SO_3: 0.03%; MnO: 0.07%). The natural pH of red mud is 10.7, which, far below the standard limit of 12.5 for hazardous waste, does not classify it as such. In addition, the toxicity leaching test of red mud showed that it does not exceed any regulatory standards [33]. Based on these findings, red mud, classified as general solid waste, can be directly utilized as a resource.

Acidic Wastewater

To minimize the effect of other factors on the purification efficiency and mechanism of RM-L73 for acid mine drainage containing Mn^{2+} and Cd^{2+}, all the acidic wastewater used in the experiment was simulated using analytical-grade reagents. The heavy metal ions in the acidic wastewater, including Mn^{2+}, Cd^{2+}, Fe^{2+}, Cu^{2+}, and Zn^{2+}, were prepared using the following analytical-grade reagents: $MnSO_4 \cdot H_2O$, $3CdSO_4 \cdot 8H_2O$, $FeSO_4 \cdot 7H_2O$, $CuSO_4 \cdot H_2O$, and $ZnSO_4 \cdot 7H_2O$. The analytical-grade reagents were accurately weighed in appropriate amounts using an analytical balance

and dissolved in distilled water. The desired concentration of the wastewater for the experiment was achieved using a volumetric flask. The pH of the wastewater containing the target ion was adjusted to the required value using dilute sulfuric acid to simulate the acidity of actual acid mine drainage. All chemicals and analytical-grade reagents were purchased from Tianli Chemical Reagent Co., Ltd. (Tianjin, China), and their purities ranged from 98% to 101%.

Batch Experiments

The batch experiments were conducted with a shaking frequency of 150 rpm at a contact temperature of 25ºC, using orbital shaking. Firstly, the required contact time for the experiment was set. After shaking, the mixture was centrifuged, and the supernatant was filtered using a sand core filtration device and a 0.45 μm aqueous filter membrane to obtain the sample. The equilibrium pH (pH_e) and electric conductivity (EC) of the samples were measured using a pH meter and a conductivity meter, respectively. The concentration of target ions in the filtrate was determined using ICP-OES after adding dilute sulfuric acid dropwise. To minimize experimental errors, all experiments were performed in duplicate, and the average values were taken.

Desorption Test

A continuous desorption test method was employed to assess the effect of ion concentration changes on the desorption capacity of the adsorbent. Distilled water and an acidic solution with an initial pH of 3.0 were utilized to investigate the desorption characteristics of RM-L73 loaded with Mn^{2+} and Cd^{2+} under neutral and acidic environments, respectively. The experimental conditions for the desorption of Mn^{2+} and Cd^{2+} on RM-L73 are as follows: The initial volume was 100 mL. The initial concentration was 100 mg/L. The desorption solutions included distilled water (H_2O) and acidic solution ($pH_0 = 3.0$). The dosages of RM-L73 for Mn^{2+} and Cd^{2+} were 16 and 8 g/L, respectively. The specific volume of the supernatant was 50 mL, the number of desorption cycles was 18, and the desorption time involved 720 min of shaking followed by 720 min of stewing.

For RM-L73 and acidic wastewater that had reached adsorption equilibrium, a specific volume (V_1) of the supernatant was taken to measure the residual concentration (C_e) of the target ions at equilibrium. Then, a specific volume (V_1) of desorption solution was added to the original conical flask to ensure that the volume of the solution in the flask was restored to its initial volume (V_0). The flask was placed in a water bath shaker for further shaking. After a set period, a specific volume (V_1) of supernatant was similarly taken to measure the residual concentration (C_{e1}) of target ions. This step marked the completion of the first desorption test. Subsequently, more desorption solution was added, and the process was repeated for multiple desorption cycles. The desorption amount of the target ions in the *i*-th desorption (ΔD_{si}) was calculated using Equation (1), while the total desorption amount of the target ion caused by the *i*-th desorption (D_{si}) was calculated using Equation (2).

$$\Delta D_{si} = \frac{V_0}{m}\left[C_{ei} - C_{e(i-1)}(1-\frac{V_1}{V_0}) \right]$$
(1)

$$D_{si} = \frac{V_0}{m}\left[C_{ei} - C_{e(i-1)}(1-\frac{V_1}{V_0}) \right] + D_{s(i-1)}$$
(2)

Where, ΔD_{si} is the desorption amount of the target ion after the completion of the *i*-th desorption experiment, mg/g; V_0 is the initial volume of solution in the desorption test, L; V_1 is the volume of the supernatant taken after the desorption test is completed, L; C_{ei} is the concentration of target ions after the *i*-th desorption test, mg/L; D_{si} is the total desorption amount of the target ion after the completion of the *i*-th desorption test, mg/g.

Competitive Adsorption Test

To prevent preferential adsorption due to differences in initial concentrations of heavy metal ions, the initial concentrations in each multi-component system were standardized in the competitive adsorption test [34]. The experimental conditions for competitive adsorption of Mn^{2+} and Cd^{2+} on RM-L73 were as follows: Mn^{2+} and Cd^{2+} were target ions, and Cu^{2+}, Zn^{2+}, and Fe^{2+} were competing ions. The initial concentration was 100 mg/L, the dosage of RM-L73 was 12 g/L, the contact time was 600 min, and the pH_0 was 3.0.

Adding coexisting ions in binary and ternary systems, which are not the target ions, leads to competition for the limited adsorption sites and effective components on RM-L73. This competition deprives the target ion of the necessary effective adsorption sites and thereby hinders its complete adsorption. Consequently, the removal efficiency and the adsorption capacity of RM-L73 for the target ion decrease, as reported by Putro et al. [35]. The mutual interference effect of coexisting ions on the competitive adsorption of target ions by RM-L73 was investigated using competitive adsorption evaluation parameters [36], which were calculated from Equation (3):

$$E = \frac{q_e'}{q_e}$$
(3)

Where, E is the competitive adsorption evaluation parameter for competitive adsorption systems; q_e' is the equilibrium adsorption capacity of target ions in a multi-component system with coexisting ions, mg/g; q_e is the equilibrium adsorption capacity of target ions in a binary system without coexisting ions, mg/g.

Microscopic Test

XPS

The compressed sample was placed into the sample chamber. The sample was then sent into the analysis chamber when the pressure was less than 2.0×10^{-7} mbar with a spot size of 400 μm, a working voltage of 12 kV, and a filament current of 6 mA. The narrow spectrum was scanned with an energy of 50 eV using a step size of 0.1 eV.

Results and Discussion

Desorption Characteristics of Mn²⁺ and Cd²⁺ on RM-L73

Desorption Characteristics of Mn²⁺ *and* Cd²⁺ *in a Neutral Environment*

Fig. 1 shows the desorption test results of Mn²⁺ and Cd²⁺ on RM-L73 under a neutral environment, respectively. Fig. 1a and Fig. 1c) illustrate the relationship between the pH_e and EC of the solution and the desorption cycles. Fig. 1b) and Fig. 1d) depict the relationship between the single desorption amount of target ions and the equilibrium concentration of the target ions after a single desorption with the desorption cycles.

Fig. 1a) and Fig. 1c) show that during the desorption under a neutral environment, the pH_e of the solutions containing Mn²⁺ and Cd²⁺ exhibited a decreasing trend with an increase in desorption cycles. This phenomenon was attributed to adding a neutral solution in each desorption test, where distilled water diluted the existing free alkaline substances in the solution. After the 18th desorption cycle, the pH_e of the solution containing Mn²⁺ dropped from 8.8 to 7.9, whereas the pH_e of the solution containing Cd²⁺ fluctuated between 7.6 and 8.1, which was within the neutral range of 6.5 to 8.5 [37]. This result may be attributed to the fact that the alkaline substances remaining in RM-L73 could continue to be released and maintain the pH of the solution within a stable range. Furthermore, with the increase in desorption cycles, the EC of the solution containing Mn²⁺ and Cd²⁺ initially decreased sharply and then stabilized at a constant value when the desorption test was completed. This phenomenon indicates that the concentration of free ions in the solution was diminishing. When the pH_e of the solution was below about 8.2, ions continued to be released from RM-L73 to maintain the pH_e and EC of the solution with minimal fluctuations due to the continuous release and reaction of inexhaustible alkaline substances in RM-L73.
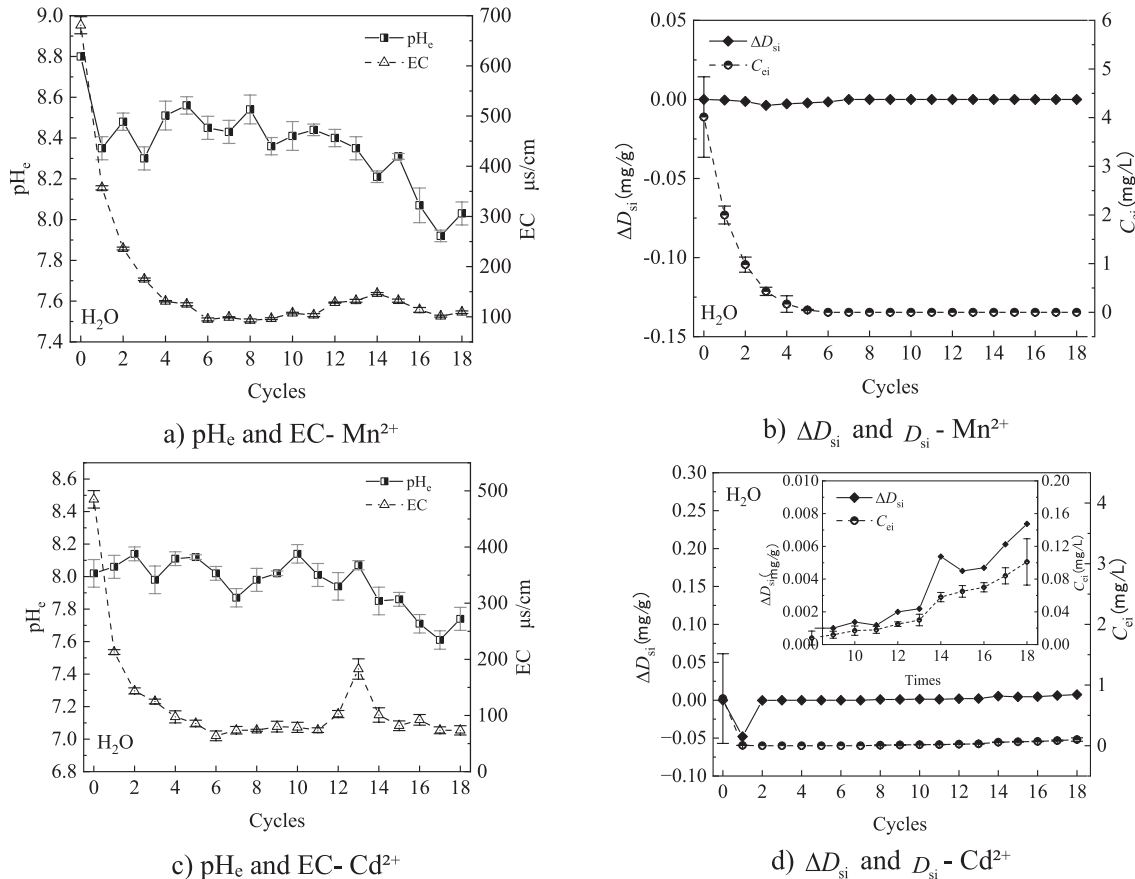

a) pH_e and EC- Mn²⁺

b) ΔD_{si} and D_{si} - Mn²⁺

c) pH_e and EC- Cd²⁺

d) ΔD_{si} and D_{si} - Cd²⁺

Fig. 1. The desorption of Mn²⁺ and Cd²⁺ on RM-L73 in a neutral environment (H_2O).

As illustrated in Fig. 1b), with the increase in desorption cycles, the desorption amount of Mn^{2+} in a neutral environment was nearly negligible, and the equilibrium concentration of Mn^{2+} consistently remained below the detection threshold. Mn^{2+} is not readily re-released from RM-L73 in a neutral environment, which minimizes the risk of secondary environmental pollution. Fig. 1d) reveals that during the initial desorption, Cd^{2+} exhibited re-adsorption, potentially due to the relatively low concentration of Cd^{2+} after adsorption (0.8 mg/L) and sufficient unoccupied adsorption sites on RM-L73, which allowed for the adoption of a small amount of Cd^{2+} upon dilution. As the desorption cycles increased, the equilibrium concentration of Cd^{2+} in a neutral environment exhibited a gradually increasing trend. After the 9th desorption cycle was completed, Cd^{2+} began to be desorbed, and when the 18th desorption cycle was completed, the concentration of Cd^{2+} approached 0.1 mg/L. Compared with Mn^{2+}, RM-L73 loaded with Cd^{2+} might have lower safety and stability in a neutral environment.

*Desorption Characteristics of* Mn^{2+}
and Cd^{2+} *in an Acidic Environment*

Fig. 2 shows the desorption test results of Mn^{2+} and Cd^{2+} on RM-L73 under an acidic environment,

respectively. Fig. 2a) and Fig. 2c) illustrate the relationship between the pH_e and EC of the solution and the desorption cycles. Fig. 2b) and Fig. 2d) depict the relationship between the single desorption amount of target ions and the equilibrium concentration of the target ions after a single desorption with the desorption cycles.

Fig. 2a) and Fig. 2c) show that as the desorption cycles increased, the pH_e of the solutions containing Mn^{2+} and Cd^{2+} significantly decreased after the first desorption cycle, followed by a trend of gradual decline. The pH_e of the solution containing Mn^{2+}, once stabilized, ranged from 7.7 to 8.3, indicating that RM-L73 loaded with Mn^{2+} and Cd^{2+} could still effectively improve and enhance the pH of acidic wastewater. Two reasons explain the decrease in pH_e: On the one hand, the free alkaline substances already present in the original solution were neutralized and diluted by the acidic desorption solution. On the other hand, the re-adsorption of Mn^{2+} and Cd^{2+} by RM-L73 during the initial desorption occurred. However, it was observed that the pH_e of the solution remained within the neutral to alkaline range after desorption. This result indicates that RM-L73, loaded with Mn^{2+} and Cd^{2+}, could still effectively improve and enhance the pH of acidic wastewater. The inexhaustible carbonate minerals, such as calcite in RM-L73, continued interacting with
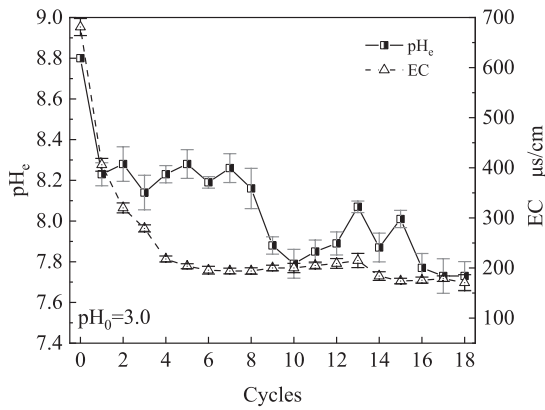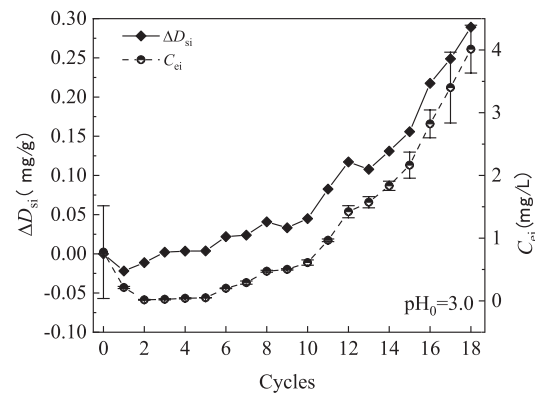

a) pH_e and EC- Mn^{2+}
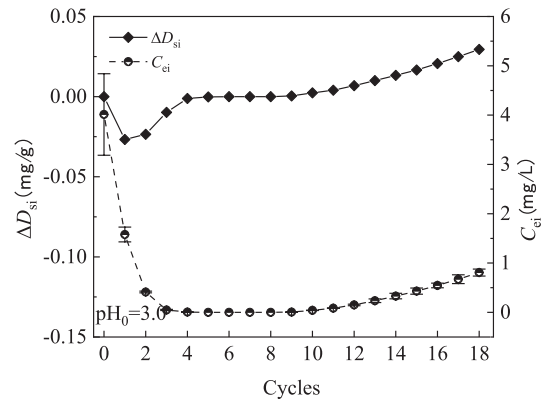
b) ΔD_{si} and D_{si} - Mn^{2+}
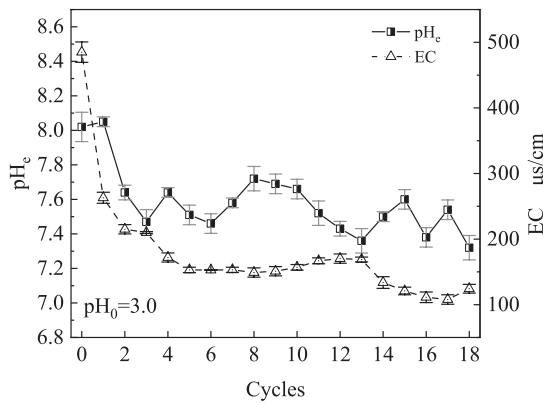
c) pH_e and EC- Cd^{2+}

d) ΔD_{si} and D_{si} - Cd^{2+}

Fig. 2. The desorption of Mn^{2+} and Cd^{2+} on RM-L73 in an acidic environment (pH_0 = 3.0).

acidic substances in the solution, thereby maintaining their alkalinity [33]. In addition, with the increase of desorption cycles, the EC of solutions containing Mn^{2+} and Cd^{2+} first sharply decreased and then stabilized. However, the EC of the solution was higher than that in neutral desorption environments, potentially owing to the RM-L73 releasing other ions in acidic environments.

In the previous desorption cycles, Mn^{2+} and Cd^{2+} exhibited varying degrees of re-adsorption on RM-L73, which may have been due to the re-exposure and opening of unoccupied adsorption sites on RM-L73 loaded with Mn^{2+} or the dissolution of surface precipitates on RM-L73 loaded with Cd^{2+} by acidic desorption solution and thereby exposed new adsorption sites. As the desorption cycles increased, the equilibrium concentrations of Mn^{2+} and Cd^{2+} gradually increased. After the 18th desorption cycle, the concentrations of Mn^{2+} and Cd^{2+} in the solution reached 0.8 and 4.0 mg/L, respectively. This result suggests that the application of RM-L73 in acidic environments must consider the environmental risks associated with the desorption of Mn^{2+} and Cd^{2+}.

Capture Mechanism of RM-L73

The capture mechanism of Mn^{2+} and Cd^{2+} in acidic wastewater by RM-L73 was further investigated using XPS.

Fig. 3 depicts the XPS spectra of RM-L73 loaded with Mn^{2+} and Cd^{2+}. After C1s calibration and peak splitting processing, the peak at Mn $2p_{3/2}$ was mainly studied. Mn^{2+} may have been oxidized to higher valence states such as Mn^{3+} or Mn^{4+}, yet Mn^{2+} remained the predominant valence state adsorbed onto RM-L73. The oxidation of Mn^{2+} may have been facilitated by a catalytic reaction upon contact with O_2, which was provided by RM-L73 in an alkaline environment [38]. The adsorption of Mn^{2+} onto RM-L73 was primarily attributed to the forming of new complexes between the non-protonated hydroxyl groups on the surface

of RM-L73 and Mn^{2+} [39]. After C1s calibration and peak splitting processing, the peak at Cd $3d_{3/2}$ was mainly analyzed. The strong peak detected at a binding energy of 405.56 eV indicated that Cd^{2+} may have undergone complexation reactions with the hydroxyl (-OH) and deprotonated state (O^-) on the surface of RM-L73. Furthermore, Cd^{2+} was adsorbed onto RM-L73 in the form of $CdCO_3$ and $Cd(OH)_2$ [40, 41].

Parameterization of Desorption Isotherms

Fig. 4 shows the desorption characteristic curves of RM-L73 loaded with Mn^{2+} and Cd^{2+} in neutral and acidic environments. The desorption isotherms of Mn^{2+} and Cd^{2+} on RM-L73 were analyzed by the Herry adsorption model [42]. The slope of the isotherm, which is the desorption distribution coefficient, a parameter introduced to characterize the ease of desorption of ions, could be used to characterize the adsorption strength of the adsorbent for target ions. Table 1 lists the relevant parameters of the desorption isotherms of Mn^{2+} and Cd^{2+} in neutral and acidic environments.

The desorption distribution coefficients for Mn^{2+} and Cd^{2+} in neutral and acidic environments were negative due to the strong adsorption properties of RM-L73 for Mn^{2+} and Cd^{2+}, as well as the low initial adsorption equilibrium concentrations of these ions in the solution. Desorption caused the adsorbed target ions to desorb from RM-L73 and thereby released them back into the solution as free ions. As previously analyzed, the adsorption mechanism of RM-L73 for Mn^{2+} and Cd^{2+} involved strong chemical adsorption of these ions by the mineral components, such as aluminosilicate minerals and calcite in RM-L73.

However, the speciation of heavy metal cations is greatly affected by pH, and the unstable speciation of the target ion in acidic environments is more likely to be re-released into the solution as an ion [43]. The ease of desorption of Mn^{2+} and Cd^{2+} in neutral and acidic

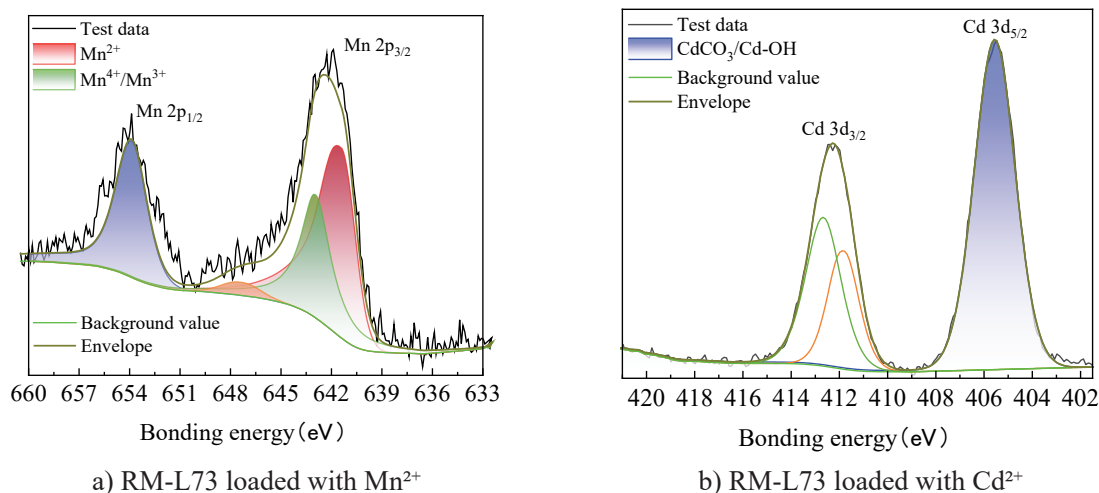a) RM-L73 loaded with Mn^{2+}

b) RM-L73 loaded with Cd^{2+}

Fig. 3. XPS spectra of RM-L73 loaded with Mn^{2+} and Cd^{2+}.

a) acidic environment (H_2O)- Mn^{2+}

b) neutral environment (H_2O) - Cd^{2+}

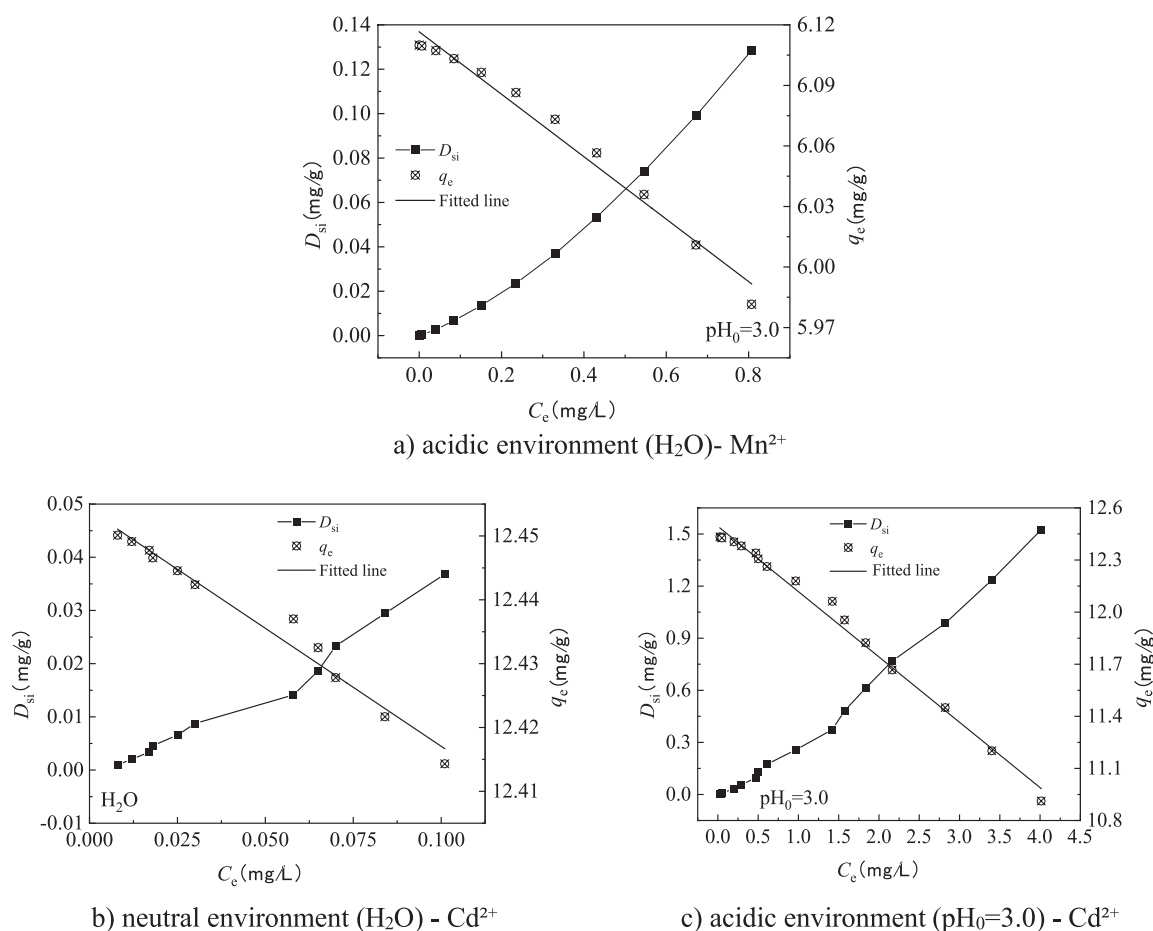c) acidic environment (pH_0=3.0) - Cd^{2+}

Fig. 4. Desorption characteristic curve of Mn^{2+} and Cd^{2+} on RM-L73 (1440 min, H_2O/ pH_0=3.0).

environments was evaluated using the desorption distribution coefficient. The larger the coefficient, the more difficult it is for RM-L73 to facilitate the desorption of the target ion. For Cd^{2+}, which was successfully adsorbed by RM-L73, desorption was more likely to occur in acidic environments than in neutral ones. Mn^{2+} did not undergo desorption in a neutral environment; however, a slight desorption phenomenon was observed in acidic environments. Based on the desorption distribution coefficient of Mn^{2+} and Cd^{2+} in acidic environments, Mn^{2+} was more difficult to desorb and release after being adsorbed on RM-L73 compared with Cd^{2+}.

Competitive Adsorption Characteristics of Mn^{2+} and Cd^{2+} on RM-L73

Competitive Adsorption Parameters of Mn^{2+} and Cd^{2+}

Table 2 presents the competitive adsorption evaluation parameters of Mn^{2+} and Cd^{2+} in different initial concentrations of single, binary, and ternary systems.

The E values of Mn^{2+} and Cd^{2+} were generally less than 1 in binary and ternary systems, indicating an antagonistic effect of coexisting ions on their adsorption.

For Mn^{2+}, the minimum E value was generally observed at an initial concentration of 100 mg/L. As the initial concentration further increased, the E of Mn^{2+} slightly increased. It indicates that in high-concentration competitive adsorption systems, the antagonistic effect of coexisting ions on Mn^{2+} was weak. For Cd^{2+}, a gradually decreasing trend was observed as the initial concentration increased. At the lower initial concentration stage, sufficient adsorption sites and active components were available for Cd^{2+} and coexisting ions due to the large dosage of RM-L73, which ensured complete adsorption. Therefore, the antagonistic effect of coexisting ions was not evident and created an illusion of no interaction. However, as the initial concentration increased, coexisting ions competed with the Cd^{2+} for effective adsorption sites on RM-L73, which led to a reduced adsorption capacity and a clear inhibitory effect.

Adsorption Capacity of Mn^{2+} and Cd^{2+} in a Competitive Adsorption System

The Langmuir isotherm adsorption model was employed to determine the maximum adsorption capacity for Mn^{2+} and Cd^{2+} in the competitive adsorption tests [44, 45]. The variations in the maximum adsorption capacity of RM-L73 for Mn^{2+} and Cd^{2+} in binary

Table 1. Characteristic parameters of desorption curves of Mn^{2+} and Cd^{2+} on RM-L73.

Desorption method	Ion type	Desorption solution	Desorption distribution coefficient	R^2
Continuous	Mn^{2+}	Neutral solution (H_2O)	-	-
		Acidic solution ($pH_0 = 3.0$)	-0.15	0.9791
	Cd^{2+}	Neutral solution (H_2O)	-0.36	0.9732
		Acidic solution ($pH_0 = 3.0$)	-0.38	0.9907

Table 2. E of Mn^{2+} and Cd^{2+} in single, binary, and ternary systems.

System	Target ion (-coexisting ions)	E				
		Initial concentration (mg/L)				
		25	50	100	150	200
Mn^{2+} as the target ion						
Single	Mn^{2+}	1	1	1	1	1
Binary	Mn^{2+}-Cd^{2+}	0.9392	0.7510	0.5342	0.5864	0.7017
	Mn^{2+}-Cu^{2+}	0.9911	0.8652	0.5654	0.5152	0.2200
	Mn^{2+}-Zn^{2+}	1	0.9413	0.6437	0.6507	0.6766
	Mn^{2+}-Fe^{2+}	0.9590	0.8852	0.6444	0.7002	0.6818
Ternary	Mn^{2+}-Cd^{2+}-Cu^{2+}	0.8803	0.5449	0.3527	0.4599	0.3901
	Mn^{2+}-Cd^{2+}-Zn^{2+}	0.9385	0.6174	0.4037	0.4767	0.5227
	Mn^{2+}-Cd^{2+}-Fe^{2+}	0.9678	0.6926	0.3947	0.4823	0.5211
Cd^{2+} as the target ion						
Single	Cd^{2+}	1	1	1	1	1
Binary	Cd^{2+}-Mn^{2+}	1	0.9990	0.9546	0.8979	0.8565
	Cd^{2+}-Cu^{2+}	0.9943	0.9960	0.9468	0.7353	0.5054
	Cd^{2+}-Zn^{2+}	0.9950	0.9967	0.9855	0.8336	0.6729
	Cd^{2+}-Fe^{2+}	0.9948	0.9968	0.9483	0.7851	0.5320
Ternary	Cd^{2+}-Mn^{2+}-Cu^{2+}	0.9912	0.9761	0.8527	0.6893	0.5409
	Cd^{2+}-Mn^{2+}-Zn^{2+}	0.9825	0.9788	0.8734	0.6961	0.5459
	Cd^{2+}-Mn^{2+}-Fe^{2+}	0.9942	0.9852	0.8666	0.7103	0.5566

and ternary systems, which consist of the target ion and different coexisting ions, are illustrated in Fig. 5. Table 3 presents the basic physicochemical parameters of H^+, Mn^{2+}, Cd^{2+}, Cu^{2+}, Zn^{2+}, and Fe^{2+}.
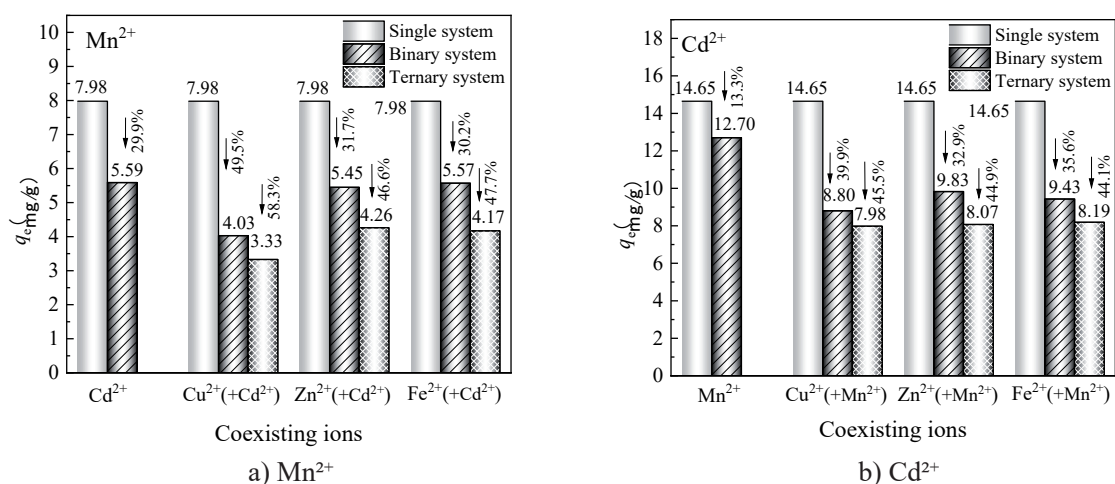
Fig. 5 shows the Langmuir adsorption capacity of RM-L73 for Mn^{2+} and Cd^{2+} in single, binary, and ternary systems. Compared with the maximum adsorption capacity of RM-L73 for the Mn^{2+} and Cd^{2+} in the single system, the adsorption capacity of Mn^{2+} and Cd^{2+} in the binary system was significantly reduced due to the presence of coexisting ions. The adsorption capacities of Mn^{2+} decreased by 29.9% to 49.5%, whereas Cd^{2+} decreased by 13.3% to 39.9%. The antagonistic effect order of coexisting ions for Mn^{2+} was $Cu^{2+}>Zn^{2+}>Fe^{2+}>Cd^{2+}$. For Cd^{2+}, the antagonistic effect order was

$Cu^{2+}>Fe^{2+}>Zn^{2+}>Mn^{2+}$. In the ternary system, with the addition of another coexisting ion, the competition between the Mn^{2+} and the adsorption sites and active ingredients on RM-L73 was further intensified. The adsorption capacities of Mn^{2+} on RM-L73 decreased by 46.6% to 58.3%, and Cd^{2+} decreased by 44.1% to 45.5%. In the ternary system where Mn^{2+} and Cd^{2+} coexist, the antagonistic effect order of the third coexisting ion affecting Mn^{2+} was $Cu^{2+}>Fe^{2+}>Zn^{2+}$, and for Cd^{2+} was $Cu^{2+}>Zn^{2+}>Fe^{2+}$. Cu^{2+} exhibited the greatest antagonistic effect on Mn^{2+} and Cd^{2+}. Table 3 shows Cu^{2+} had the smallest hydrated ion radius and a large charge size ratio. Smaller hydrated ion radii correspond to lower migration resistance of heavy metal ions, which is characteristic of preferential adsorption. Moreover, the larger the charge

Table 3. Basic physicochemical parameters of each ion in the acidic wastewater.

Ion type	Effective ionic radius (pm)	Electronegativity	pK_1	Hydrated ion radius (nm)	Charge size ratio
H^+	-	2.20	-	0.282	-
Mn^{2+}	67	1.55	10.59	0.438	2.99
Cd^{2+}	95	1.69	9.2	0.426	2.11
Cu^{2+}	73	1.90	7.34	0.419	2.74
Zn^{2+}	74	1.65	8.96	0.430	2.70
Fe^{2+}	78	1.83	6.8	0.428	2.56

Fig. 5. Langmuir adsorption capacity of Mn^{2+} and Cd^{2+} in single, binary, and ternary systems.

size ratio, the stronger the bond energy. Furthermore, a larger charge size ratio indicates stronger bond energy. Therefore, Cu^{2+} significantly influenced and reduced the adsorption effect of RM-L73 on target ions in binary and ternary systems [46].

Comparing the decrease in maximum adsorption capacity of Mn^{2+} and Cd^{2+} shows that the coexisting ions Cu^{2+}, Zn^{2+}, and Fe^{2+} exerted a greater antagonistic effect on Mn^{2+} than Cd^{2+}. These coexisting ions possibly severely inhibited the adsorption of Mn^{2+} by RM-L73. This can be attributed to the significantly smaller hydrated ion radius of Cd^{2+} compared with that of Mn^{2+}. With a smaller hydrated ion radius, Cd^{2+} is more easily bound to RM-L73 particles than Mn^{2+}, which resulted in a weaker antagonistic effect. When RM-L73 is used to purify acidic wastewater containing Mn^{2+}, the potential degradation in Mn^{2+} removal efficiency due to coexisting ions must be considered, although desorption experiments revealed that the speciation of Mn^{2+} on RM-L73 after purification is relatively stable compared with Cd^{2+}.

Conclusions

In this study, the safety and effectiveness of the RM-L73 were investigated. The desorption characteristics

of Mn^{2+} and Cd^{2+} on RM-L73 under neutral and acidic environments were examined through continuous desorption tests. Additionally, the competitive adsorption characteristics of Mn^{2+} and Cd^{2+} on RM-L73 in the presence of coexisting ions in binary and ternary systems were explored. The main conclusions drawn are as follows:

(1) RM-L73 loaded with Mn^{2+} does not exhibit desorption of Mn^{2+} in neutral environments, but it does in acidic environments. Conversely, RM-L73 loaded with Cd^{2+} can undergo desorption of Cd^{2+} in neutral and acidic environments, and the desorption strength of Cd^{2+} is greater in acidic environments than in neutral ones. The desorption behaviors of Mn^{2+} and Cd^{2+} in neutral and acidic environments can be effectively described by the desorption distribution coefficient. In practical applications, considering and monitoring changes in the pH levels of the RM-L73 service environment, as well as replacing the active media in a timely manner, are essential to prevent secondary environmental pollution. Moreover, RM-L73 possesses a great buffering capacity for acidic wastewater.

(2) The antagonistic effect of coexisting ions on the adsorption of Mn^{2+} and Cd^{2+} in binary and ternary systems was determined through competitive adsorption evaluation parameters. As the initial concentration increases, the antagonistic effect of coexisting ions

on the adsorption is generally enhanced. The effective adsorption sites and active components on RM-L73 are competed for and occupied by coexisting ions, which hinders the adsorption of the target ions and reduces the adsorption capacity of RM-L73 for them.

(3) In the binary system, the antagonistic effect order of Cd^{2+}, Cu^{2+}, Zn^{2+}, and Fe^{2+} on Mn^{2+} is $Cu^{2+}>Zn^{2+}>Fe^{2+}>Cd^{2+}$. For the antagonistic effect on Cd^{2+}, the order is $Cu^{2+}>Fe^{2+}>Zn^{2+}>Mn^{2+}$. In the ternary system, the antagonistic effect order of Cu^{2+}, Zn^{2+}, and Fe^{2+} on Mn^{2+} is $Cu^{2+}>Fe^{2+}>Zn^{2+}$. Similarly, the antagonistic effect order on Cd^{2+} is $Cu^{2+}>Zn^{2+}>Fe^{2+}$. The antagonistic effect order of coexisting ions on target ions in different adsorption systems correlates with the charge size ratio and the hydrated ion radius of the ions.

(4) The adsorption effectiveness of RM-L73 on Mn^{2+} and Cd^{2+} in binary and ternary systems is significantly affected and reduced by the presence of Cu^{2+}, which has the smallest hydrated ion radius and a large charge size ratio. Furthermore, the adsorption of Mn^{2+} is more susceptible to the antagonistic effects of coexisting ions than that of Cd^{2+}.

Acknowledgments

Conflict of Interest

The authors declare no conflict of interest.

References

1. MOODLEY I., SHERIDAN C.M., KAPPELMEYER U., AKCIL A. Environmentally sustainable acid mine drainage remediation: Research developments with a focus on waste/by-products. Minerals Engineering, **126**, 207, **2018**.

2. NAIDU G., RYU S.C., THIRUVENKATACHARI R., CHOI Y.K., JEONG S.H., VIGNESWARAN S. A critical review on remediation, reuse, and resource recovery from acid mine drainage. Environmental Pollution, **247**, 1110, **2019**.

3. LI Z.Y., MA Z.W., VAN DER KUIJP T.J., YUAN Z.W., HUANG L. A review of soil heavy metal pollution from mines in China: pollution and health risk assessment. Science of the Total Environment, **468**, 843, **2014**.

4. GONZÁLEZ Á., DEL MAR GIL-DIAZ M., DEL CARMEN LOBO M. Metal tolerance in barley and wheat cultivars: physiological screening methods and application in phytoremediation. Journal of Soils and Sediments, **17** (5), 1403, **2016**.

5. WANG Z.L., XU Y.X., ZHANG Z.X., ZHANG Y.B. Review: Acid mine drainage (AMD) in abandoned coal mines of Shanxi, China. Water, **13** (8), 1, **2021**.

6. MHLONGO S.E., AMPONSAH-DACOSTA F. A review of problems and solutions of abandoned mines in South Africa. International Journal of Mining, Reclamation and Environment, **30** (4), 279, **2015**.

7. REZAIE B., ANDERSON A. Sustainable resolutions for environmental threat of the acid mine drainage. Science of the Total Environment, **717**, 137211, **2020**.

8. ALQADAMI A.A., WABAIDUR S.M., JEON B.H., KHAN M.A. Co-hydrothermal valorization of food waste: process optimization, characterization, and water decolorization application. Biomass Conversion and Biorefinery, **14**, 15757, **2024**.

9. ALI I., ALHARBI O.M.L., ALOTHMAN Z.A., ALWARTHAN A., AL-MOHAIMEED A.M. Preparation of a carboxymethylcellulose-iron composite for uptake of atorvastatin in water. International Journal of Biological Macromolecules, **132**, 244, 2019.

10. SIVASANKARAPILLAI V.S., BASKARAN S., SUNDARARAJAN A., SIDDIQUI M.R., WABAIDUR S.M., MUTHUKRISHNAN A., DHANUSURAMAN R. Porous network of nitrogen self-doped honeycomb like activated carbon derived from Caladium tricolor leaves: a multifunctional platform for energy and environmental applications. Journal of Porous Materials, **31**, 1489, **2024**.

11. ANSARI N., ALI A., AKHTAR M.S., HASAN S., KHATOON T., KHAN A.R., WABAIDUR S.M., RAHMAN Q.I. Green synthesis of zinc oxide marigold shaped clusters using Eucalyptus globulus leaf extract as robust photocatalyst for dyes degradation under sunlight. Materials Science in Semiconductor Processing, **173**, 108087, **2024**.

12. ALI I., ALHARBI O.M.L., ALOTHMAN Z.A., Al-MOHAIMEED A.M., ALWARTHAN A. Modeling of fenuron pesticide adsorption on CNTs for mechanistic insight and removal in water. Environmental Research, **170**, 389, **2019**.

13. ZHENG Q. The study on mechanism of the treatment of acid mine drainage using PRB with loess-steel slag, Taiyuan University of Technology, Taiyuan, China, **2020**.

14. LV X. Study on the influence of coal mine goaf water on the water ecological environment of Yangquan Shandi basin and its prevention and control countermeasures, Shanxi University, Taiyuan, China, **2021**.

15. CHEN H.L., ZHENG J., ZHANG Z.Q., LONG Q., ZHANG Q.Y. Application of annealed red mud to Mn^{2+} ion adsorption from aqueous solution. Water Science and Technology, **73** (11), 2761, **2016**.

16. NECULITA C.M., ROSA E. A review of the implications and challenges of manganese removal from mine drainage. Chemosphere, **214**, 491, **2019**.

17. PURKAYASTHA D., MISHRA U., BISWAS S. A comprehensive review on Cd(II) removal from aqueous solution. Journal of Water Process Engineering, **2**, 105, **2014**.

18. YANG T.X., WANG Y.F., SHENG L.X., HE C.G., SUN W., HE Q. Enhancing Cd(II) sorption by red mud with heat treatment: Performance and mechanisms of sorption. Journal of Environmental Management, **255**, 109866, **2020**.

19. VAN H.T., NGUYEN L.H., NGUYEN V.D., NGUYEN X.H., NGUYEN T.H., NGUYEN T.V., VIGNESWARAN S., RINKLEBE J., TRAN H.N. Characteristics and mechanisms of cadmium adsorption onto biogenic

aragonite shells-derived biosorbent: Batch and column studies. Journal of Environmental Management, **241**, 535, **2019**.

20. LIU M.H., LV Z.H., CHEN Z.H., YU S.C., GAO C.J. Comparison of reverse osmosis and nanofiltration membranes in the treatment of biologically treated textile effluent for water reuse. Desalination, **281**, 372, **2011**.

21. FU W., JI G.Z., CHEN H.H., YANG S.Y., GUO B., YANG H., HUANG Z.Q. Molybdenum sulphide modified chelating resin for toxic metal adsorption from acid mine wastewater. Separation and Purification Technology, **251**, 117407, **2020**.

22. TENG W.K., LIU G.L., LUO H.P., ZHANG R.D., XIANG Y.B. Simultaneous sulfate and zinc removal from acid wastewater using an acidophilic and autotrophic biocathode. Journal of Hazardous Materials, **304**, 159, **2016**.

23. KONG L.H., SHI C.H., MA F.S., ZHOU B. Comparison of treatment on SBR tail water in tidal flow constructed wetlands with different packing. Chinese Journal of Environmental Engineering, **11** (1), 379, **2017**.

24. MITTAL A., NAUSHAD M., SHARMA G., ALOTHMAN Z.A., WABAIDUR S.M., ALAM M. Fabrication of MWCNTs/ThO_2 nanocomposite and its adsorption behavior for the removal of Pb(II) metal from aqueous medium. Desalination and Water Treatment, **57** (46), 21863, **2016**.

25. KHAN M.A., WABAIDUR S.M., SIDDIQUI M.R., ALQADAMI A.A., KHAN A.H. Silico-manganese fumes waste encapsulated cryogenic alginate beads for aqueous environment de-colorization. Journal of Cleaner Production, **244**, 118867, **2020**.

26. AZAM M., WABAIDUR S.M., KHAN M.R., AL-RESAYES S.I., SHAHIDULISLAM M. Heavy metal ions removal from aqueous solutions by treated ajwa date pits: Kinetic, isotherm, and thermodynamic approach. Polymers, **14** (5), 914, **2018**.

27. LI Y.C., HUANG H., XU Z., MA H.Q., GUO Y.F. Mechanism study on manganese(II) removal from acid mine wastewater using red mud and its application to a lab-scale column. Journal of Cleaner Production, **253**, 119955, **2020**.

28. ZHAO L.N., QIN Z., LI X.B., YE J.J., CHEN J.Y. Adsorption of Cu(II) by phosphogypsum modified with sodium dodecyl benzene sulfonate. Journal of Hazardous Materials, **387**, 121808, **2020**.

29. SABAH M.A., ABDEL K.M.A. From waste to waste: iron blast furnace slag for heavy metal ions removal from aqueous system. Environmental Science and Pollution Research International, **29** (38), 57964, **2022**.

30. LU Y.S., LIU X.F., XIE M.X., YU L.Y., DONG X.Q. Synergistic purification of acid mine drainage containing Cd(II) by red mud and loess. Science Technology and Engineering, **23** (7), 3091, **2023**.

31. LU Y.S., LIU X.F., YU L.Y., ZHANG X.D., DUAN W., PARK J.B., DONG X.Q. Removal characteristics and mechanism of Mn(II) from acidic wastewater using red mud-Loess mixture. Polish Journal of Environmental Studies, **31** (6), 5781, **2022**.

32. SANDER M., PIGNATELLO J.J. On the reversibility of sorption to black carbon: distinguishing true hysteresis from artificial hysteresis caused by dilution of a competing adsorbate. Environmental Science & Technology, **41** (3), 843, **2007**.

33. LU Y.S., LIU X.F., ZHANG H., LI J.S. Purification of acidic wastewater containing Cd(II) using a red mud–loess mixture: Column test, breakthrough curve, and speciation of Cd. Water Science and Technology, **89** (12), 3252, **2024**.

34. SHAHROKHI-SHAHRAKI R., BENALLY C., EL-DIN M.G., PARK J. High efficiency removal of heavy metals using tire-derived activated carbon vs commercial activated carbon: Insights into the adsorption mechanisms. Chemosphere, **264** (1), 128455, **2021**.

35. PUTRO J.N., SANTOSO S.P., ISMADJI S., JU Y.-H. Investigation of heavy metal adsorption in binary system by nanocrystalline cellulose–bentonite nanocomposite: Improvement on extended Langmuir isotherm model. Microporous and Mesoporous Materials, **246**, 166, **2017**.

36. MAHAMADI C., NHARINGO T. Competitive adsorption of Pb^{2+}, Cd^{2+} and Zn^{2+} ions onto Eichhornia crassipes in binary and ternary systems. Bioresource Technology, **101** (3), 859, **2010**.

37. Standard for groundwater quality. GB/T 14848-2017, General Administration of Quality Supervision, Inspection and Quarantine of the People's Republic of China/ Standardization Administration of the People's Republic of China, China.

38. HUANG H., LI Y.C., XU Z., XIAO H.Z., REN B.Z. Removal of Mn^{2+} from wastewater by red mud and its mechanism analysis. Bulletin of the Chinese Ceramic Society, **38**, 2801, **2019**.

39. TANG Y.C., HU W., XU M.T., HUANG X.H., LI W.H., YANG Y.Y., QIAN Y.Q. Mechanism study on the Mn^{2+} removal from water by oxidation an adsorption with $KMnO_4$. Environmental Science & Technology, **41**, 31, **2018**.

40. MA W.Y., PEI P.G., GAO G., SUN Y.B. Structural characteristics of micro-nano particle size biochar and its adsorption mechanism for Cd^{2+}. Environmental Science, **43**, 3682, **2022**.

41. YIN G.C., TAO L., CHEN X.L., BOLAN N.S., SARKAR B., LIN Q.T., WANG H.L. Quantitative analysis on the mechanism of Cd^{2+} removal by $MgCl_2$-modified biochar in aqueous solutions. Journal of Hazardous Materials, **420**, 126487, **2021**.

42. WANG Y.Z. Soils modification for liners and service life analysis, Zhejiang University, Hangzhou, China, **2014**.

43. TESSIER A., CAMPBELL P.G.C. BISSON M., Sequential extraction procedure for the speciation of particulate trace metals. Analytical Chemistry, **51** (7), 844, **1979**.

44. ALOTHMAN Z.A., BAHKALI A.H., KHIYAMI M.A., ALFADUL S.M., WABAIDUR S.M., ALAM M., ALFARHAN B.Z. Low cost biosorbents from fungi for heavy metals removal from wastewater. Separation Science and Technology, **55** (10), 1766, **2020**.

45. KENAWY EI-R. G., GHFAR A.A., WABAIDUR S.M., KHAN M.A., SIDDIQUI M.R., ALOTHMAN Z.A., ALQADAMI A.A., HAMI M. Cetyltrimethylammonium bromide intercalated and branched polyhydroxystyrene functionalized montmorillonite clay to sequester cationic dyes. Journal of Environmental Management, **219**, 285, **2018**.

46. NIGHTINGALE JR E.R. Phenomenological theory of ion solvation. Effective radii of hydrated ions. Journal of Physical Chemistry, **63** (9), 1381, **1959**.